ChemComm

COMMUNICATION

View Article Online
View Journal | View Issue

Cite this: *Chem. Commun.*, 2016, 52, 2764

Received 10th November 2015,
Accepted 4th January 2016

DOI: 10.1039/c5cc09173j

www.rsc.org/chemcomm

Edge-rich and dopant-free graphene as a highly efficient metal-free electrocatalyst for the oxygen reduction reaction†

Li Tao,‡[a] Qiang Wang,‡[b] Shuo Dou,[a] Zhaoling Ma,[a] Jia Huo,[a] Shuangyin Wang*[a] and Liming Dai*[c]

For the first time, we developed edge-rich and dopant-free graphene as a highly efficient ORR electrocatalyst. Electrochemical analysis revealed that the as-obtained edge-rich graphene showed excellent ORR activity through a one-step and four-electron pathway. With a similar strategy, edge-rich carbon nanotubes and graphite can also be obtained with enhanced ORR activity. This work confirms the important role of edge carbon in efficient ORR electrocatalysis without interruption by any other dopants.

As a key process in fuel cells and metal-air batteries, the oxygen reduction reaction (ORR) has significantly limited the commercialization of these devices due to its poor reaction kinetics.[1] Previous researches indicated that the ORR could proceed in two ways: an efficient one-step, four-electron pathway and a two-step, two-electron pathway.[2] The state-of-the-art electrocatalysts for the ORR are Pt-based noble metal catalysts due to their good capability to catalyze the ORR.[3] However, Pt suffers from major drawbacks of high cost, CO poisoning and poor stability, which limit its large-scale application.[4] Towards this end, the development of efficient and inexpensive catalysts for the ORR is of top importance. Numerous studies have been performed to design and prepare metal-free or precious-metal-free electrocatalysts for the ORR.[5] Fe–N/C complex electrocatalysts have been extensively reported as noble-metal-free electrocatalysts for the ORR.[6] On the other hand, total metal-free electrocatalysts were also demonstrated to show good ORR performance, such as heteroatom-doped carbon.[7]

The heteroatom doping into carbon nanomaterials (including graphene and carbon nanotubes) could efficiently tune the electronic properties, surface structure, and thus the electrochemical performance.[8] Depending on the type of the heteroatom and its interaction with the bulk carbon atoms, the ORR mechanism on doped carbon by different heteroatoms may slightly vary.[9] Previously, we have reported N-doped carbon nanotubes, B and N co-doped carbon, and S-doped graphene as highly efficient metal-free electrocatalysts for the ORR with an ideal four-electron and one-step reaction pathway.[10] Other groups also performed systematic research on doped carbon based metal-free electrocatalysts for the ORR.[11] All of these studies demonstrate the important role of the heteroatoms. However, the exact mechanism of the ORR on doped carbon is still controversial. In spite of these conditions, we may figure out from the amounts of literature reports that the induced charge polarization of carbon atoms by the heteroatoms may significantly contribute to the improved ORR performance.[11,12] Alternatively, the search for other strategies to induce the charge polarization of carbon atoms without heteroatom doping may be a promising possibility.[13] Recently, we have demonstrated by a self-designed micro-droplet electrochemical system that the edge of graphite is much more active for the ORR than the basal plane due to the charge polarization of edge carbon atoms.[14] Meanwhile, Hu *et al.* also proves the contribution of defects of carbon for the ORR.[15] Therefore, it is fundamentally important to discover the electrocatalytic behavior of edge-rich and dopant-free carbon and technically promising to develop an efficient strategy to produce edge-rich carbon electrocatalysts.

In this work, we, for the first time, developed dopant-free and edge-rich graphene as a highly efficient metal-free electrocatalyst for the ORR. As shown in Scheme 1, by appropriately controlling the temperature and treatment time, the edge sites on the basal plane of the graphene surface significantly increased. The edge-rich properties of graphene may be able to show advanced electrocatalytic performance for the ORR, as we proved that the edge of carbon is more active than the basal plane. Our physical characterization verified this viewpoint, and the electrochemical analysis further revealed that the as-obtained edge-rich graphene showed higher ORR activity than the pristine one in terms of the onset potential and current density due to the increased edge sites. More importantly, the absence of dopants in the catalyst could provide an ideal model to focus on the contribution of the edge carbon atom during

[a] *State Key Laboratory of Chem/Bio-Sensing and Chemometrics, College of Chemistry and Chemical Engineering, Hunan University, Changsha, 410082, P. R. China. E-mail: shuangyinwang@hnu.edu.cn*
[b] *Department of Applied Chemistry, Nanjing Tech University, Nanjing, 211816, China*
[c] *Department of Macromolecular Science and Engineering Case Western Reserve University, Cleveland, OH 44106, USA. E-mail: liming.dai@case.edu*

† Electronic supplementary information (ESI) available. See DOI: 10.1039/c5cc09173j

‡ These authors contributed to this work equally.

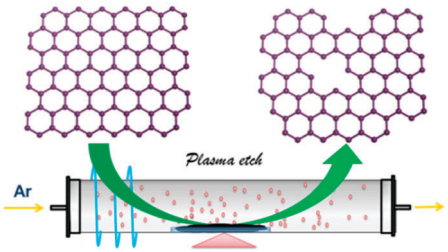

Scheme 1 Illustration of the preparation of the edge-rich and dopant-free graphene by Ar plasma etching.

ORR electrocatalysis. In order to verify the feasibility of this facile strategy, few-layer carbon nanotubes and graphite were also etched by Ar plasma with the aim of generating more edges in CNTs as active sites for the ORR. Consistent with our hypothesis, the ORR performance of few-layer carbon nanotubes and graphite could be obviously enhanced in the presence of more edges, in spite of the absence of dopants.

Graphene was prepared from graphite oxide by thermal expansion to get a volume-fluffy structure, which could improve the accessibility with the generated ion/electron by plasma to make the etching more efficient. Fig. 1 shows the SEM and TEM images of the graphene before and after Ar plasma etching for 1 h at 700 °C. As shown by the SEM images of pristine graphene (denoted as G) and plasma-treated graphene (denoted as P–G) in Fig. 1a and b, both the kinds of graphene show similar macroscopic surface morphology, indicating that Ar plasma treatment did not cause serious structural damage on graphene with the ideal electronic conductivity reserved. On the other hand, the resolution of SEM is not enough to precisely and clearly observe the change in the graphene layer. Subsequently, TEM images of the two samples were collected, as shown in Fig. 1c and d. It can be seen that the pristine graphene shows a smooth surface; however, there are many holes with a diameter of around 15 nm on the plasma-treated graphene. According to Fig. 1d and the inset graph, nanosized holes were generated by the plasma treatment, while the macroscopic structure of graphene was still reserved. This interesting structure would provide enriched active sites and reserve the good electrical conductivity of graphene, which are beneficial for ORR electrocatalysis. The X-ray diffraction (XRD) patterns of the samples of G and P–G are shown in Fig. S1 (ESI†). Compared with pristine graphene, the plasma treated graphene has the same characteristic peaks, and the (002) peak reveals a similar FWHM and peak intensity. These results indicate that plasma treated graphene has a similar structure to pristine graphene.

Raman spectroscopy is an efficient tool to investigate the surface electronic properties of carbon-based materials.[16] Typical features of carbon materials in Raman spectra are the G-band at around 1590 cm^{-1} and the D-band at around 1350 cm^{-1}. The intensity ratio of D to G bands, I_D/I_G, could reflect the defect level of carbon materials.[17] Fig. S2 (ESI†) displays the Raman spectra of two samples excited by a 632 nm laser. As seen from the curves, after plasma treatment, the value of I_D/I_G increased from 1.16 to 1.51, indicating the increase of the defects in the graphene surface. This result indicated that the plasma treatment could significantly increase the defect sites by generating holes and edges.

X-ray photoelectron spectroscopy (XPS) was used to analyze the composition and the chemical state of G and P–G samples (Fig. 2a and b), and the C1s spectrum deconvolution analysis was carried out on the core level spectra of characteristic elements in the samples.[18] In the survey spectra (Fig. 2a), both the C1s and O1s peaks were observed, and the presence of oxygen species may be due to the physical adsorption of oxygen. It is well-known that there are two kinds of carbon atoms in graphene, namely, the basal-plane sp^2 carbon atoms and the defect sp^3 carbon atoms. So, the sp^3 level reflects the defect degree of graphene. Fig. 2b shows the peaks of C1s in plasma treated and untreated (or pristine) graphene thin films. The C1s peak can be mainly deconvoluted into five sub-peaks at 284.75, 285.90, 286.90, 287.70 and 289.51 eV, which can be assigned to C–C (sp^2), "defect peak" (sp^3), C–O, C═O and shakeup π–π* satellite, respectively (the result of de-convolution of the C1s peaks displayed in Table S1, ESI†).[19] Compared to G, the ratio of sp^2/sp^3 of P–G decreased from 8.88 to 6.35, and the percentage of the sp^3 carbon increased in P–G relative to G, indicating the presence of more defects and edges in P–G. These XPS results are consistent with the Raman and HRTEM characterization, and all these characterization results confirmed the successful preparation of edge-rich graphene with more edges/defects by Ar plasma etching. Therefore, the significantly enhanced electrocatalytic

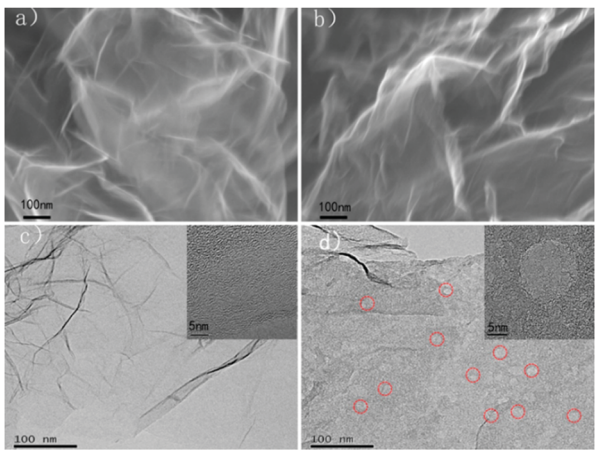

Fig. 1 SEM images of pristine graphene (a) and Ar plasma treated graphene (b); TEM images of pristine graphene (c) and Ar plasma treated graphene (d), the inset graph of (c) and (d) are the HRTEM of pristine and are plasma treated graphene.

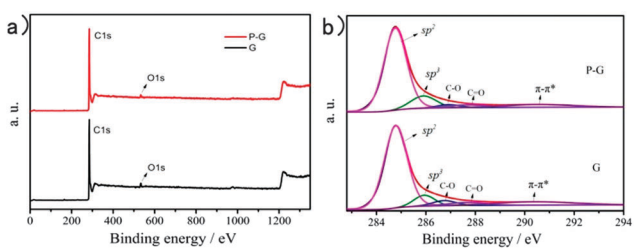

Fig. 2 XPS survey spectra (a) and C1s spectra of G and P–G (b).

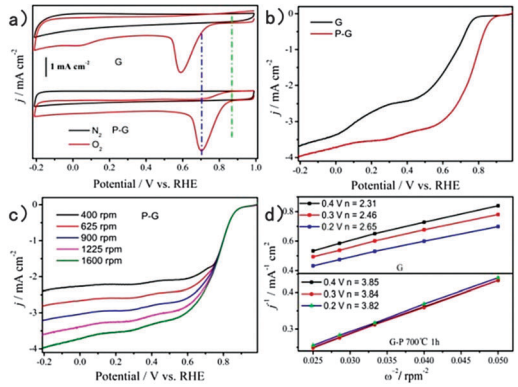

Fig. 3 Cyclic voltammograms of G and P–G at a scan rate of 50 mV s^{-1} in N_2-saturated and O_2-saturated aqueous solutions of 0.1 M KOH (a); rotating disk electrode (RDE) voltammograms of G and P–G in an O_2-saturated 0.1 M KOH solution with a scan rate of 10 mV s^{-1} (b); rotating disk electrode (RDE) of P–G at different rotation rates from 400 to 1600 rpm (c); Koutecky–Levich plots for G and P–G from 0.2 V to 0.4 V (d).

activity for the ORR on the as-obtained edge-rich graphene may be expected, as discussed below.

To investigate the electrocatalytic activity towards the ORR of the samples, the cyclic voltammogram (CV) curves were collected with a three-electrode system in alkaline medium. Fig. 3a shows the CVs of G and P–G in N_2-saturated and O_2-saturated 0.1 M KOH solution, and both the electrodes showed a substantial reduction process in the presence of oxygen. As observed, the onset potential of the ORR on the untreated graphene electrode is at 0.76 V (*vs.* RHE) with the cathodic reduction peak at around 0.59 V (*vs.* RHE). In contrast, the onset potential and reduction peak of the edge-rich graphene (P–G) shifted positively to around 0.87 and 0.70 V (*vs.* RHE). The shift of the onset potential and the reduction peak potential of the ORR clearly demonstrated a significant enhancement in the ORR electrocatalytic activity of the edge-rich graphene relative to the pristine graphene electrode.

To further investigate the kinetics of the ORR on pristine graphene and edge-rich graphene, linear sweep voltammetric (LSV) measurements were carried out on a rotating disk electrode (RDE) coated with G and P–G. Fig. 3b shows the LSV polarization curves of P–G and G measured at a rotation rate of 1600 rpm, indicating that the ORR onset potential on the P–G electrode (0.912 V) was more positive than that on G (0.806 V). The half-wave potential (*i.e.*, the potential at which the current is half of the limiting current) of the ORR on the P–G electrode is about 0.737 V, which is much more positive than the pristine G (0.572 V). At the same time, the limiting diffusion current density at −0.21 V of G–P was slightly higher than that of G. The LSV results clearly demonstrate that the ORR activity on graphene could be significantly enhanced by increasing the active edge sites by plasma etching. It should be mentioned that the ORR activity of the edge-rich graphene (P–G) is still not as good as the commercial Pt/C, as evidenced in Fig. S3 (ESI†). But the as-proposed strategy to develop edge-rich carbon is promising for the design of metal-free electrocatalysts for the ORR.

The transferred electron number (n) per oxygen molecule involved in the oxygen reduction was used to further quantitatively characterize G and P–G electrodes, which were calculated by the Koutecky–Levich equation (see ESI†).[10] As shown in Fig. 3d, the electron transfer number of G and P–G from the slopes of Koutecky–Levich plots at 0.4 V is calculated to be 2.31 and 3.85, respectively. The higher electron transfer number of the ORR on P–G than that on G indicates more efficient reaction kinetics (one-step and four-electron pathway) of the ORR on the edge-rich graphene.

In addition, we also investigated the effect of the plasma treatment time and the heating temperature during the synthesis of edge-rich graphene on the electrocatalytic activity towards the ORR. Fig. S4a (ESI†) shows the LSV curves of the edge-rich graphene obtained by plasma etching at different temperatures, in which all the samples were irradiated for 1 h. With the increase of the temperature from 300 °C to 700 °C, a more positive onset potential and larger limiting diffusion current were observed. When we further increased the temperature to 800 °C, edge-rich graphene shows a similar electrocatalytic activity towards the sample obtained at 700 °C, indicating that a further temperature increase would not significantly affect the ORR performance of edge-rich graphene. With the increase of temperature, the system energy was increased, and with the higher energy, the more active edges will be obtained. Graphene was also treated for different time periods at 700 °C. As shown in Fig. S4b (ESI†), initially, with the increase of the treatment time, the edge-rich graphene shows gradually increased ORR activity, indicating that longer treatment time may lead to more edges generated in edge-rich graphene. However, the further increase of the treatment time to 1.5 h results in slightly poorer ORR activity than that treated for 1 h, probably caused by the over-treatment of graphene resulting in poor electrical conductivity. Raman spectra (Fig. S5, ESI†) verified it. The above control experiment shows that the performance of edge-rich graphene is strictly sensitive to the temperature and plasma treatment time.

The edge-rich graphene electrode was further subjected to testing the possible crossover effect and the stability towards the ORR. In order to examine the possible methanol crossover effect of P–G, the current–time (i–t) chronoamperometric responses for the ORR at the P–G and Pt/C electrodes were conducted. As shown in Fig. S6 (ESI†), a sharp decrease in current upon addition of 1.0 M methanol at 150 s on the Pt/C electrode was observed. However, the corresponding amperometric response on the P–G electrode remained almost unchanged after the addition of methanol. This observation indicates that the P–G electrocatalyst has unambiguous fuel selectivity towards the ORR compared to the commercial Pt/C electrocatalyst. On the other hand, the durability testing of the P–G electrode was conducted at 0.74 V in an O_2-saturated 0.1 M KOH solution. As seen in Fig. S5b (ESI†), after 20 000 s the P–G electrode caused only a slight loss (12%) of current density before leveling off. In contrast, the corresponding current loss on the Pt/C electrode under the same conditions is as high as about 29%. These results clearly indicate that the catalytically active sites on the plasma treated edge-rich graphene are much more stable than those on the commercial Pt/C electrode.

Furthermore, in order to validate the universality of edge-rich carbon by plasma etching for the ORR, we treated the few-layer carbon nanotubes and graphite with Ar plasma for 1 h at 700 °C. To observe the surface change of the few-layer carbon nanotubes (CNTs) before and after Ar plasma etching (P-CNTs),

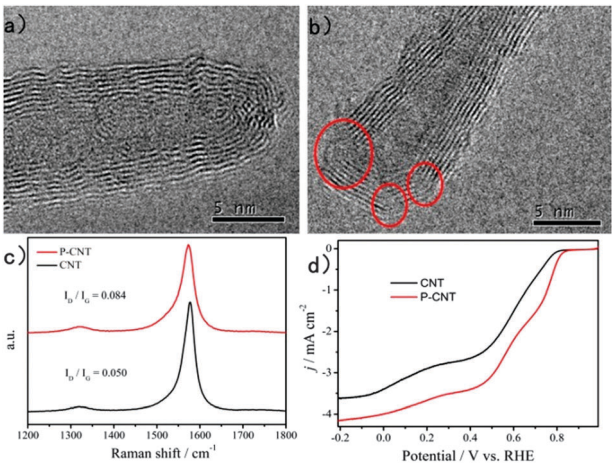

Fig. 4 TEM of pristine carbon nanotubes (a) and Ar plasma treated carbon nanotubes (b); Raman characterization of CNTs and P-CNTs (c); RDE voltammograms of pristine and plasma treated edge-rich carbon nanotubes in an O_2-saturated 0.1 M aqueous KOH solution with a scan rate of 10 mV s^{-1} (d).

HRTEM images were collected, as shown in Fig. 4a and b. Compared with the complete tubular structure of CNTs, the P-CNTs show many lattice cracks and defects on the walls of carbon nanotubes. In addition, Fig. 4c displays the Raman spectra of two samples (CNTs and P-CNTs), and the value of I_D/I_G increased from 0.050 for CNTs to 0.084 for P-CNTs, indicating the increase of defects. Both the HRTEM and Raman characterization results confirm that the edge-rich carbon nanotubes were successfully obtained by plasma etching. Fig. 4d shows the LSV polarization curves of the ORR on CNTs and P-CNTs, the ORR onset potential on the P-CNT electrode (at 0.83 V) was more positive than that of pristine CNTs (at 0.79 V). The Raman characterization and LSV testing displayed the same result as the P-CNTs (Fig. S7, ESI†). The LSV testing demonstrates that the ORR activity on CNTs and graphite could be significantly enhanced by enriching the edges by Ar plasma treatment. This observation for edge-rich CNTs and graphite is consistent with that for edge-rich graphene, confirming the important role of edges in ORR electrocatalysis and indicating the universality of plasma etching to generate edge-rich carbon nanomaterials. The plasma treated graphene was also compared with other metal-free doped carbon materials and it displayed comparable oxygen reduction ability (Table S2, ESI†).

Finally, in order to unveil the ORR mechanism on edge-rich graphene, we performed the density functional theory (DFT) calculations on graphene with or without holes, as shown in Fig. S8 (ESI†). It could be seen from the charge distribution of carbon atoms of graphene that the basal plane carbon carries negligible charge, and higher charge densities were observed on the edge carbon. According to previous reports, the carbon atoms with large charge density are most likely to serve as catalytically active sites.[14,20] Fig. S6 (ESI†) also illustrates that the edge-rich graphene shows larger oxygen adsorption energy. Therefore, the edge-rich graphene with higher charge densities could provide more active sites than the pristine graphene to catalyze the ORR.

In summary, we, for the first time, developed edge-rich and dopant-free graphene, CNTs and graphite as efficient metal-free electrocatalysts for the ORR with superior performance. The plasma etching increased the active edge sites on the carbon surface plane to facilitate the ORR catalytic activity. Notably, the edge-rich graphene electrode shows remarkable ORR electrocatalytic activities with better fuel selectivity and higher long-term stability than that of the commercially available Pt/C electrode. Our physical characterization results indicated that the edge-rich graphene maintains an integrity structure without causing serious damage on the macroscopic structure caused by the plasma treatment. Overall, this work confirms the important role of edge carbon in efficient ORR electrocatalysis without interruption by any other dopants. This work successfully demonstrates that the excellent ORR performance of carbon-based metal-free electrocatalysts could be realized by designing edge-rich carbon materials even without doping. Furthermore, it is expected that the ORR performance could be further enhanced by doping heteroatoms into the edge-rich carbon catalysts with the combined contribution of heteroatom doping and the edge effect. This finding provides a novel design principle of metal-free electrocatalysts.

This work was supported by National Natural Science Foundation of China (Grant No. 51402100, 21573066, and 21373112).

Notes and references

1 K. Gong, F. Du, Z. Xia, M. Durstock and L. Dai, *Science*, 2009, **323**, 760–764.
2 D. Geng, Y. Chen, Y. Chen, Y. Li, R. Li, X. Sun, S. Ye and S. Knights, *Energy Environ. Sci.*, 2011, **4**, 760–764.
3 S. Sun, F. Jaouen and J. P. Dodelet, *Adv. Mater.*, 2008, **20**, 3900–3904.
4 L. Qu, Y. Liu, J. B. Baek and L. Dai, *ACS Nano*, 2010, **4**, 1321–1326.
5 Y. Li, Y. Zhao, H. Cheng, Y. Hu, G. Shi, L. Dai and L. Qu, *J. Am. Chem. Soc.*, 2012, **134**, 15–18; Y. Zhao, C. Hu, L. Song, L. Wang, G. Shi, L. Dai and L. Qu, *Energy Environ. Sci.*, 2014, **7**, 1913–1918.
6 Y. Zhu, B. Zhang, X. Liu, D.-W. Wang and D. S. Su, *Angew. Chem., Int. Ed.*, 2014, **53**, 10673–10677.
7 S. Yang, X. Feng, X. Wang and K. Müllen, *Angew. Chem., Int. Ed.*, 2011, **50**, 5339–5343.
8 H. Wang, T. Maiyalagan and X. Wang, *ACS Catal.*, 2012, **2**, 781–794; Q. Wang, X. Wang, Z. Chai and W. Hu, *Chem. Soc. Rev.*, 2013, **42**, 8821–8834.
9 D. W. Wang and D. Su, *Energy Environ. Sci.*, 2014, **7**, 576–591.
10 S. Wang, E. Iyyamperumal, A. Roy, Y. Xue, D. Yu and L. Dai, *Angew. Chem., Int. Ed.*, 2011, **50**, 11756–11760; S. Wang, L. Zhang, Z. Xia, A. Roy, D. W. Chang, J. B. Baek and L. Dai, *Angew. Chem., Int. Ed.*, 2012, **51**, 4209–4212; Z. Ma, S. Dou, A. Shen, L. Tao, L. Dai and S. Wang, *Angew. Chem., Int. Ed.*, 2015, **127**, 1908–1912.
11 Z. H. Sheng, H. L. Gao, W. J. Bao, F. B. Wang and X. H. Xia, *J. Mater. Chem.*, 2012, **22**, 390–395.
12 L. Zhang and Z. Xia, *J. Phys. Chem. C*, 2011, **115**, 11170–11176; G. Kuanping, D. Feng, X. Zhenhai, D. Michael and D. Liming, *Science*, 2009, **323**, 760–764.
13 S. Dou, A. Shen, L. Tao and S. Wang, *Chem. Commun.*, 2014, **50**, 10672–10675; S. Wang, D. Yu, L. Dai, D. W. Chang and J. B. Baek, *ACS Nano*, 2011, **5**, 6202–6209.
14 A. Shen, Y. Zou, Q. Wang, R. A. W. Dryfe, X. Huang, S. Dou, L. Dai and S. Wang, *Angew. Chem.*, 2014, **126**, 10980–10984.
15 Y. Jiang, L. Yang, T. Sun, J. Zhao, Z. Lyu, O. Zhuo, X. Wang, Q. Wu, J. Ma and Z. Hu, *ACS Catal.*, 2015, **5**, 6707–6712.
16 K. N. Kudin, B. Ozbas, H. C. Schniepp, R. K. Prud'homme, I. A. Aksay and R. Car, *Nano Lett.*, 2008, **8**, 36–41.
17 C. Casiraghi, A. Hartschuh, H. Qian, S. Piscanec, C. Georgi, A. Fasoli, K. S. Novoselov, D. M. Basko and A. C. Ferrari, *Nano Lett.*, 2009, **9**, 1433–1441.
18 H. Estrade-Szwarckopf, *Carbon*, 2004, **42**, 1713–1721.
19 R. Haerle, E. Riedo, A. Pasquarello and A. Baldereschi, *Phys. Rev. B: Condens. Matter Mater. Phys.*, 2002, **65**, 321–325.
20 L. Zhang, J. Niu, M. Li and Z. Xia, *J. Phys. Chem. C*, 2014, **118**, 3545–3553; L. Zhang and Z. Xia, *J. Phys. Chem. C*, 2011, **115**, 11170–11176.